

This is the accepted manuscript made available via CHORUS. The article has been published as:

Surface vibrational modes of the topological insulator Bi_2Se_3 observed by Raman spectroscopy

H.-H. Kung, M. Salehi, I. Boulares, A. F. Kemper, N. Koirala, M. Brahlek, P. Lošťák, C. Uher, R. Merlin, X. Wang, S.-W. Cheong, S. Oh, and G. Blumberg

Phys. Rev. B **95**, 245406 — Published 9 June 2017

DOI: [10.1103/PhysRevB.95.245406](https://doi.org/10.1103/PhysRevB.95.245406)

Surface vibrational modes of the topological insulator Bi_2Se_3 observed by Raman spectroscopy

H.-H. Kung,^{1,*} M. Salehi,^{1,2} I. Boulares,³ A. F. Kemper,⁴ N. Koirala,¹ M. Brahlek,¹
P. Lošťák,⁵ C. Uher,³ R. Merlin,³ X. Wang,^{1,6} S.-W. Cheong,^{1,6} S. Oh,¹ and G. Blumberg^{1,7,†}

¹*Department of Physics & Astronomy, Rutgers University, Piscataway, NJ 08854, USA*

²*Department of Materials Science and Engineering,
Rutgers University, Piscataway, NJ 08854, USA*

³*Department of Physics, University of Michigan, Ann Arbor, Michigan 48109-1040, USA*

⁴*Department of Physics, North Carolina State University, Raleigh, North Carolina 27695, USA*

⁵*Faculty of Chemical Technology, University of Pardubice,
Studentska 573, 53210 Pardubice, Czech Republic*

⁶*Rutgers Center for Emergent Materials, Rutgers University, Piscataway, NJ 08854, USA*

⁷*National Institute of Chemical Physics and Biophysics, 12618 Tallinn, Estonia*

We present polarization resolved Raman scattering study of surface vibration modes in the topological insulator Bi_2Se_3 single crystal and thick films. Besides the 4 Raman active bulk phonons, we observed 4 additional modes with much weaker intensity and slightly lower energy than the bulk counterparts. Using symmetry analysis, we assigned these additional modes to out-of-plane surface phonons. Comparing with first principle calculations, we conclude that the appearance of these modes is due to c -axis lattice distortion and van der Waals gap expansion near the crystal surface. Two of the surface modes at 60 and 173 cm^{-1} are associated with Raman active A_{1g} bulk phonon modes, the other two at 136 and 158 cm^{-1} are associated with infrared active bulk phonons with A_{2u} symmetry. The latter become Raman allowed due to reduction of crystalline symmetry from D_{3d} in the bulk to C_{3v} on the crystal surface. In particular, the 158 cm^{-1} surface phonon mode shows a Fano lineshape under resonant excitation, suggesting interference in the presence of electron-phonon coupling of the surface excitations.

I. INTRODUCTION

Topological insulators (TIs) are a new class of quantum matter characterized by linearly dispersed spin polarized gapless surface states within the bulk band gaps [1–8], which may lead to realization of novel phenomena and applications such as spintronics and quantum computing [8–17].

Despite the topological protection, the surface states away from the Dirac point suffer from hexagonal warping effect, resulting in increased scattering rate at the TI surface [18–20]. Among many possible inelastic scattering mechanisms, electron-phonon interaction is especially important due to its direct impact on device applications at finite temperature [21, 22]. In particular, the self-energies and symmetries of the surface vibrational modes are essential for modeling the possible relaxation channels of the surface state excitations.

Theoretical modeling of surface lattice dynamics was first developed by Lifshitz and Rosenzweig [23, 24], and later expanded by various workers [25–28]. The basic idea is to consider the free surface as a perturbation of an infinite lattice, and therefore to derive the surface modes from the spectrum of bulk vibrations. As a result, the frequencies of atomic vibration modes at the surface are modified to a smaller value than in the

bulk at the Brillouin zone center (Γ point). If there is a gap in the phonon density-of-state (DOS) and with large enough distortion, the surface phonon DOS can be entirely separated from the bulk [23, 26]. Such modes are long lived and localized at the surface, where the dispersion can be quite different than the bulk [29]. However, it is often experimentally challenging to distinguish surface signal from the overwhelmingly stronger intensity contribution of the bulk. Moreover, if the surface vibration mode is not completely gapped out from the bulk spectrum, then the surface and bulk modes are indistinguishable. Instead, the “bulk phonon” acquires only a slight energy shift near the crystal surface. Notice that the surface modes originate from abrupt termination of the lattice restoring force across bulk/vacuum interface in a semi-infinite crystal, and should not be confused with the phonons in quasi-2D ultrathin samples, which are almost decoupled from the underlying substrate of a different material [30–34].

Bi_2Se_3 is one of the most studied TI due to its relatively simple band structure, i.e., a single Dirac cone within the 0.3 eV bulk band gap, much larger than the thermal energy at the room temperature. While the bulk phonon modes have been extensively studied in Bi_2Se_3 single crystals [30, 31, 33–42], only a few papers have reported studies of the surface vibration modes. Zhu and coworkers observed strong Kohn anomaly at about $2k_F$ using helium atom scattering (HAS) [43], and deduced the interaction between surface phonon and the Dirac electrons to be much stronger than the values previously reported by angle-resolved photoemission spectroscopy

* skung@physics.rutgers.edu

† girsh@physics.rutgers.edu

TABLE I. The list of single crystal and films measured in this study.

Sample #	Composition	Description	Growth
#2	Bi ₂ Se ₃	50 QL thick film	MBE
#8	(Bi ₂ Se ₃) _m (In ₂ Se ₃) _n	50 nm superlattice with (m,n)=(5,5)	MBE
#10	(Bi ₂ Se ₃) _m (In ₂ Se ₃) _n	50 nm superlattice with (m,n)=(10,5)	MBE
#13	Bi _{1.95} In _{0.05} Se ₃	single crystal with indium doping	Bridgman
#14	Bi ₂ Se ₃	pristine single crystal	Bridgman
#A	Bi ₂ Se ₃	pristine single crystal	Bridgman

(ARPES) measurements [19, 44–46], suggesting that the electron-phonon coupling on TI surface may be more complex than anticipated. Time-resolved ARPES study of single crystals reported the observation of one A_{1g} bulk phonon at about 74 cm^{-1} , and an additional mode with slightly lower energy consistent with what was suggested by transport measurements [22]. This mode was interpreted as a surface phonon associated with the observed A_{1g} bulk phonon [47]. However, alternative results have also been reported [46, 48–50], suggesting the existence of multiple phononic decaying channels which may depend on details of sample preparation. Electron energy loss spectroscopy (EELS) study has distinguished a weak mode at about 160 cm^{-1} in Bi₂Se₃, which was assigned to the surface vibration mode associated with an A_{1g} bulk phonon [51]. The Raman scattering work on bulk single crystal [38] and exfoliated nano-crystals reported several additional features, and were attributed to infrared active phonon modes becoming Raman active due to inversion symmetry breaking at crystal surface [30, 34].

To date, different surface modes were measured by several distinct spectroscopies, with slight discrepancies between the results and interpretations. To resolve the discrepancy, it is desirable to study all surface vibration modes within one technique that provides both high energy resolution and symmetry information.

Raman spectroscopy is a conventional tool for studying surface phonon modes [52, 53]. Here, we use high resolution polarization resolved Raman spectroscopy to study the vibrational modes in Bi₂Se₃ samples. We focus our study to the bulk single crystals, which are unexposed to air or any chemicals. In addition to the 4 Raman active bulk phonons, we observed 6 additional modes with about 20–100 times weaker intensities compared to the bulk phonons (Fig. 1). By comparing the data to the results obtained by the complementary spectroscopic techniques and the calculations, we assign the observed additional modes to surface phonons arising from out-of-plane lattice distortion near the crystal/film interface.

This paper is organized as follows. In Sec. II, we introduce the experiments including sample preparations and the Raman probe. In Sec. III, we present the low temperature polarized Raman spectra of bulk and thin film Bi₂Se₃ samples. Sec. IV discusses the symmetries and microscopic views of the surface vibration modes.

Finally, we conclude our discussions in Sec. V. Details of data analysis are given in Appendix.

II. EXPERIMENTAL SETUP

Table I lists 6 Bi₂Se₃ single crystals and films measured in this study. The bulk single crystals were grown by modified Bridgman method [54, 55]. The thin film samples were epitaxially grown on Al₂O₃ (0001) substrates in a custom designed molecular beam epitaxy (MBE) chamber [56, 57]. They were immediately transferred into a cryostat after taking out of MBE chamber.

The superlattice thin films of (Bi₂Se₃)_m(In₂Se₃)_n are grown along (0001) surface [56], where each primitive cell consists of m QL Bi₂Se₃ and n QL In₂Se₃, with each QL being $\sim 1\text{ nm}$ thick. Notice that the light penetration depth in In₂Se₃ within energy range of current study is about 100 nm [58], which is about 10 times larger than the penetration depth in Bi₂Se₃ [59]. Therefore, the signal is dominated by scattering from Bi₂Se₃, and the scattering volume in the superlattice samples is practically the same as bulk.

Bi₂Se₃ has a rhombohedral crystal structure with the D_{3d} point group symmetry. The irreducible representations and Raman selection rules are given in Table II. With 5 atoms in a primitive unit cell, there are a total of 3 acoustic and 12 optical bulk phonon branches. At the Γ -point, the irreducible representations of the Raman active phonons are $2A_{1g} + 2E_g$, and the infrared active phonons are $2A_{2u} + 2E_u$ [35, 36]. These bulk phonon modes have been measured by Raman and infrared spectroscopies [30, 31, 33–42], and the values reported in Ref. [37] and Ref. [38] are listed in Table III.

The crystal naturally cleaves along the (111) surface terminated at Se atoms, forming optically flat quintuple layers (QLs) weakly bonded by van der Waals force [35]. The surface QL has the symmorphic $P6mm$ wallpaper group symmetry (two dimensional crystallographic point group C_{6v}) [60–62]. Since the surface layer phonon modes in Bi₂Se₃ are not perfectly localized and decay into the bulk, it is more appropriate to analyze our experimental results within the layer group $P3m1$ (crystallographic point group C_{3v} , which is a subgroup containing common symmetry operators of D_{3d} and C_{6v} groups) [61].

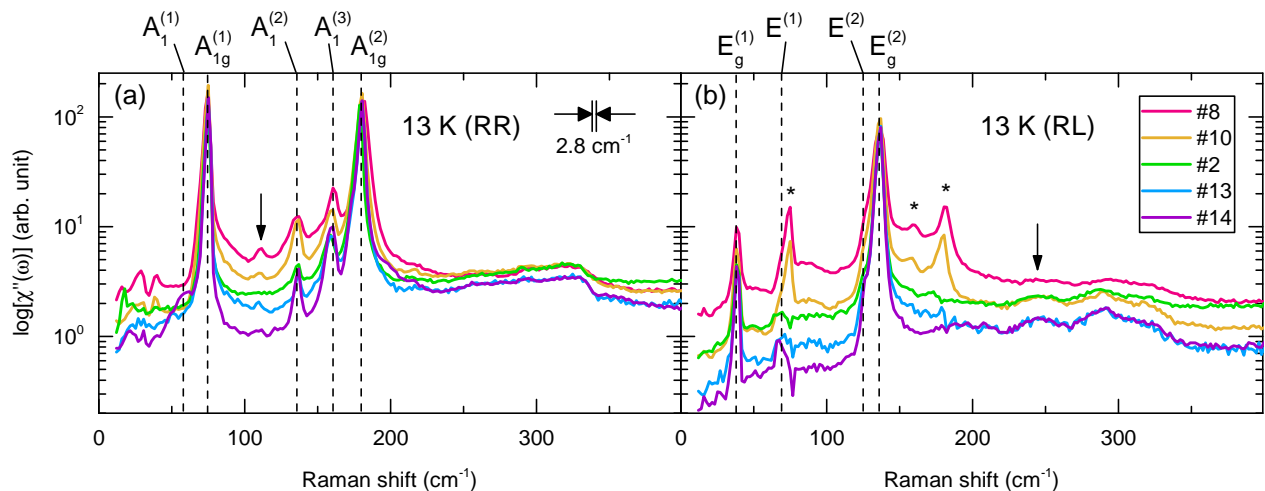


FIG. 1. (Color online) The Raman response function $\chi''(\omega)$ measured in the (a) RR and (b) RL scattering geometry at 13 K with 532 nm excitation from various Bi_2Se_3 samples as described in Table I, plot in semi-log scale. The dashed lines label the observed phonon modes as tabulated in Table III. (a) The mode at 110 cm^{-1} indicated by arrow is due to the phonon signal from $\alpha\text{-In}_2\text{Se}_3$ layers [63]. The asterisks mark the phonon modes with A_{1g} and A_1 symmetries, appear in RL geometry due to indium atom diffusion. The instrumental resolution of 2.8 cm^{-1} is shown.

158 All Raman scattering measurements are taken from
 159 ab surfaces freshly cleaved or grown immediately prior
 160 to the measurements. Sample #2–14 are measured in a
 161 quasi-backscattering geometry in a continuous He-flow
 162 optical cryostat. A glove bag with controlled dry nitro-
 163 gen gas environment was sealed to the cryostat loading
 164 port. After purging the bag to the desired conditions,
 165 the single crystals were cleaved in the glove bag immedi-
 166 ately before loading into the cryostat for cooling, without
 167 exposure to air. We use $\lambda_L = 532\text{ nm}$ solid state laser for
 168 excitation, where the spot size is roughly $50\ \mu\text{m}$. The
 169 scattered light was analyzed and collected by a custom
 170 triple-grating spectrometer equipped with a liquid nitro-
 171 gen cooled CCD detector.

172 As for the data collected from sample #A, measure-
 173 ments were done in a back-scattering geometry from
 174 a cold-finger cryostat. An argon ion laser and a
 175 Ti:Sapphire laser were used as sources, where the spot
 176 sizes are roughly 35 and $55\ \mu\text{m}$, respectively. The scat-
 177 tered light was collected using a triple stage spectrometer
 178 (Dilor XY) and imaged on a CCD camera.

179 All spectra shown were corrected for the spectral re-
 180 sponse of the spectrometer and CCD to obtain the Ra-
 181 man intensity $I_{\mu\nu}(\omega, T)$, which is related to the Ra-
 182 man response function $\chi''_{\mu\nu}(\omega, T)$ by the Bose factor
 183 $n(\omega, T)$: $I_{\mu\nu}(\omega, T) = [1 + n(\omega, T)]\chi''_{\mu\nu}(\omega, T)$. Here, μ
 184 (ν) denotes the polarization of incident (scattered) pho-
 185 ton, ω is energy and T is temperature. The scatter-
 186 ing geometries used in this experiment are denoted as
 187 $\mu\nu = RR, RL, XX$ and YX , which is short for $\bar{z}(\mu\nu)z$ in
 188 Porto's notation. $R = X + iY$ and $L = X - iY$ denotes the
 189 right- and left-circular polarizations, respectively, where
 190 X (Y) denotes linear polarization parallel (perpendicu-
 191 lar) to the plane of incidence. The irreducible represen-

192 tations of the D_{3d} and C_{3v} groups corresponding to these
 193 scattering geometries are listed in Table II. Notice that
 194 in both the D_{3d} and C_{3v} groups, the phonon intensities
 195 do not depend on the orientation of the crystallographic
 196 axis. The notations X and Y have no reference to the
 197 crystallographic a and b axes. In order to avoid confu-
 198 sion with the weak surface modes, possible polarization
 199 leakage arising from optical elements are removed from
 200 presented data with a procedure described in Appendix.

III. RESULTS

202 Figure 1 shows the Raman response function $\chi''(\omega)$,
 203 taken at 13 K with 532 nm excitation, plot in semi-log
 204 scale. In order to confirm the tiny features of surface
 205 modes, we compared the results from bulk crystals and
 206 MBE films. Fig. 1(a) and 1(b) are measured with the RR
 207 and RL scattering geometries, respectively (Table II).

TABLE II. The Raman selection rules in the bulk and on the surface of Bi_2Se_3 [64, 65]. Upon the reduction of symmetry from point group D_{3d} to C_{3v} , the A_{1g} and A_{2u} irreducible representations merge into A_1 , A_{2g} and A_{1u} merge into A_2 , E_g and E_u merge into E . [66]

Scattering geometry	Bulk (D_{3d})	Surface (C_{3v})
RR	$A_{1g} + A_{2g}$	$A_1 + A_2$
RL	$2E_g$	$2E$
XX	$A_{1g} + E_g$	$A_1 + E$
YX	$A_{2g} + E_g$	$A_2 + E$

208 The dashed lines label the observed phonons as tabu-
 209 lated in Table III. The strong modes at 72 and 174 cm^{-1}
 210 in RR scattering geometry are the bulk A_{1g} phonons of
 211 Bi_2Se_3 (Fig. 1(a)), and the strong modes centered at 37
 212 and 132 cm^{-1} in RL are the bulk E_g phonons (Fig. 1(b)),
 213 consistent with previous Raman studies [31, 38] and cal-
 214 culations [67].

215 The broad feature at about 330 cm^{-1} in RR is possi-
 216 bly due to second-order scattering of the $A_{1g}^{(2)}$ phonon,
 217 broadened due to the large downward dispersion of the
 218 phonon branch [67]. Similarly, the broad feature ob-
 219 served around 300 cm^{-1} in RL is assigned to two-phonon
 220 excitation, $A_{1g}^{(2)} + E_g^{(2)}$. The broad feature at about
 221 245 cm^{-1} (Fig. 1(b), marked by arrow) was previously
 222 assigned to the 2D stretching mode of Se atoms on the
 223 surface [68]. However, we do not observe the reported re-
 224 sponse effect of this mode with near-infrared excitation
 225 (Fig. 2). Notice that this mode energy is also consistent
 226 with the two-phonon excitation of $A_{1g}^{(2)} + E_g^{(1)}$.

227 In order to distinguish the broad features from elec-
 228 tronic origin, such as excitations from the topological sur-
 229 face states, we compared the results with indium doped
 230 Bi_2Se_3 in Fig. 1. Indium doping was shown to increase
 231 the carrier density and suppress the topological surface
 232 states in Bi_2Se_3 [56, 69]. Here, we collected data from
 233 bulk single crystals and MBE grown $\text{In}_2\text{Se}_3/\text{Bi}_2\text{Se}_3$ su-
 234 perlattices, where indium doping is achieved through dif-
 235 fusion in the superlattices [70]. In all indium doped sam-
 236 ples, the broad features show the same intensity, sug-
 237 gesting their origin unrelated to the topological surface
 238 states. This feature is slightly weaker in the superlattice
 239 sample #8, despite the first-order phonon modes are still
 240 sharp and strong. However, this is likely mainly due to
 241 the indium atom diffusion into the Bi_2Se_3 layer, which
 242 breaks the translation symmetry, and therefore further
 243 broadens the multi-phonon mode. The diffused indium
 244 atoms also lower the local crystal symmetry in the Bi_2Se_3
 245 layers, and therefore allows vibration modes with A_{1g} and
 246 A_1 symmetries to appear in the RL geometry, which is
 247 otherwise forbidden for the crystal symmetry of Bi_2Se_3
 248 (Fig. 1(b), marked by asterisks). The small feature at
 249 110 cm^{-1} in RR is due to a strong phonon of $\alpha\text{-In}_2\text{Se}_3$
 250 layers [63] (indicated by arrow in Fig. 1(a)).

252 In addition to the strong bulk first-order Raman
 253 phonons and the broad features, we see additional sharp
 254 modes that are about 20 times weaker than the bulk
 255 phonons. In Fig. 1(a), two such features at 136 and
 256 158 cm^{-1} are seen in all samples in RR scattering ge-
 257 ometry, labeled $A_1^{(2)}$ and $A_1^{(3)}$, respectively. In the bulk
 258 single crystal sample #14, we observed a mode at about
 259 60 cm^{-1} , which we label as $A_1^{(1)}$. We associate these three
 260 features with vibration modes at the crystal surface, to
 261 be discussed in the RR polarization for the Sample #14
 262 in the next section. We also noticed several sharp fea-
 263 tures below 50 cm^{-1} in sample #8 and #10 in RR, which
 264 are possibly zone folded phonons. To confirm this re-
 265 quires further studies, and is beyond the scope of this

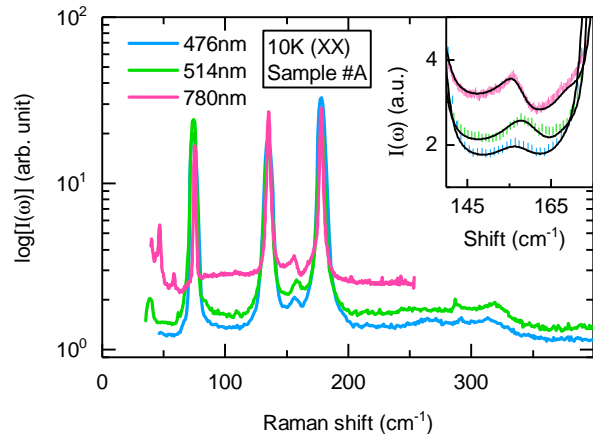


FIG. 2. (Color online) The signal intensity in the XX scattering geometry, measured at 10 K from a bulk Bi_2Se_3 single crystal, plot in semi-log scale. The blue, green and pink lines corresponds to laser excitation energy of 476, 514 and 780 nm, respectively. Inset: enlarged plot around the $A_1^{(3)}$ mode. The black lines are fit to Fano lineshape (Eq. 2).

266 paper. In the RL scattering geometry, we observed two
 267 weak features at 67 and 126 cm^{-1} , labeled $E^{(1)}$ and $E^{(2)}$,
 268 respectively (Fig. 1(b)). The energy of these modes are
 269 close to the strong bulk phonons, and therefore require
 270 higher resolution to distinguish them.

271 In Fig. 2 are the Raman spectra of the bulk sample
 272 at different excitation wavelengths at 10 K. The spectra
 273 were obtained in the XX polarization. As in Fig. 1, we
 274 observe an additional peak at 158 cm^{-1} which we refer
 275 to as $A_1^{(3)}$. However, note that the mode is more asym-
 276 metric when 780 nm excitation wavelength is used. This
 277 is an indication that the $A_1^{(3)}$ phonon is interacting with
 278 a continuum.

280 To further understand the observed phonon modes, we
 281 measure the Raman response in 4 scattering geometries
 282 of the D_{3d} and C_{3v} point group as listed in Table II
 283 (Fig. 3(a)). The intensity contributed by each symmetry
 284 channel in different scattering geometries are dictated by
 285 the Raman tensors [64, 65] and the results for D_{3d} and
 286 C_{3v} groups are listed in Table II. Therefore, by obtain-
 287 ing polarized Raman spectra in 4 proper scattering ge-
 288 ometries, we can separate the measured Raman response
 289 from each symmetry channel.

$$\begin{aligned}
 \chi''_{A_{1g}}(\omega) + \chi''_{A_1}(\omega) &= \chi''_{XX}(\omega) - \frac{1}{2}\chi''_{RL}(\omega) \\
 \chi''_{A_{2g}}(\omega) + \chi''_{A_2}(\omega) &= \chi''_{YX}(\omega) - \frac{1}{2}\chi''_{RL}(\omega) \\
 \chi''_{E_g}(\omega) + \chi''_E(\omega) &= \frac{1}{2}\chi''_{RL}(\omega)
 \end{aligned} \quad (1)$$

290 The results are shown in Fig. 3(b). We notice that no
 291 lattice vibrational mode is observed in the A_{2g} and A_2
 292 symmetry channels. This is because the Raman tensors
 293 for these two channels are antisymmetric and commonly

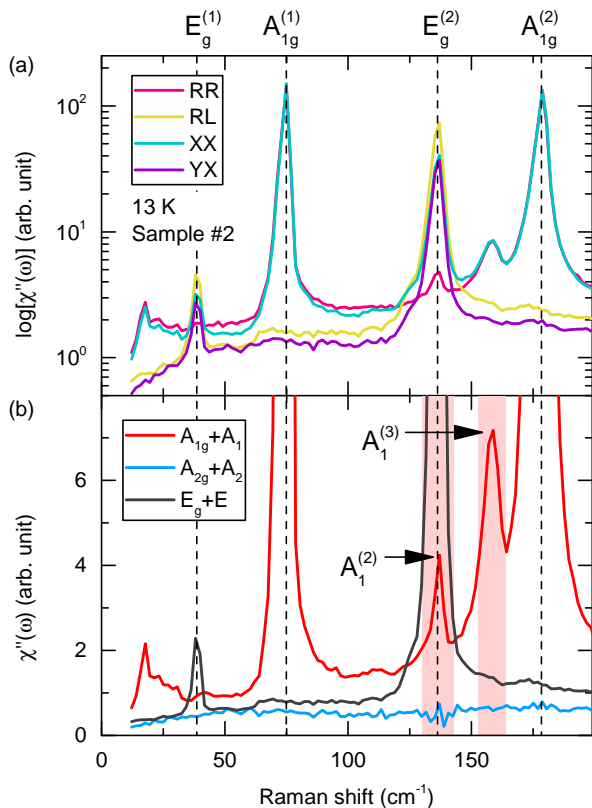


FIG. 3. (Color online) (a) The Raman spectra taken in all 4 scattering geometries at 13 K with 532 nm excitation from a Bi_2Se_3 thick film, plotted on a semi-log scale. (b) The Raman response of different symmetry channels, obtained from data in (a). The bulk phonons are marked by dashed lines, whereas the surface modes are indicated by arrows and shaded in red.

294 correspond to pseudo-vector-like excitations [64, 71, 72],
 295 which is forbidden for phononic Raman scattering in
 296 Bi_2Se_3 . Since the signal in A_{2g} and A_2 channels are expected
 297 to be zero, we can claim that all vibration modes
 298 appearing in RR have either A_{1g} or A_1 symmetry (Ta-
 299 ble II).

300 The $A_1^{(2)}$ mode happens to have energy very close to
 301 the $E_g^{(2)}$ phonon, making it particularly difficult for spectroscopic
 302 experiments to distinguish. Here, we utilize
 303 the symmetry properties to separately detect them with
 304 polarized light. The polarization leakage of optical elements
 305 are precisely measured and removed, and thereby
 306 excluding the possibility of $A_1^{(2)}$ being a trivial polarization
 307 leakage from the $E_g^{(2)}$ phonon.

308 To distinguish surface modes that are particularly
 309 weak and close in energy to the bulk phonons, we take
 310 high resolution spectra from a carefully prepared bulk
 311 crystal #14, cleaved in nitrogen environment. We show
 312 in Fig. 4 the spectra taken at 13 K in RR and RL scattering
 313 geometries, where the smoother low resolution
 314 (2.8 cm^{-1}) data is overlapped with the high resolution

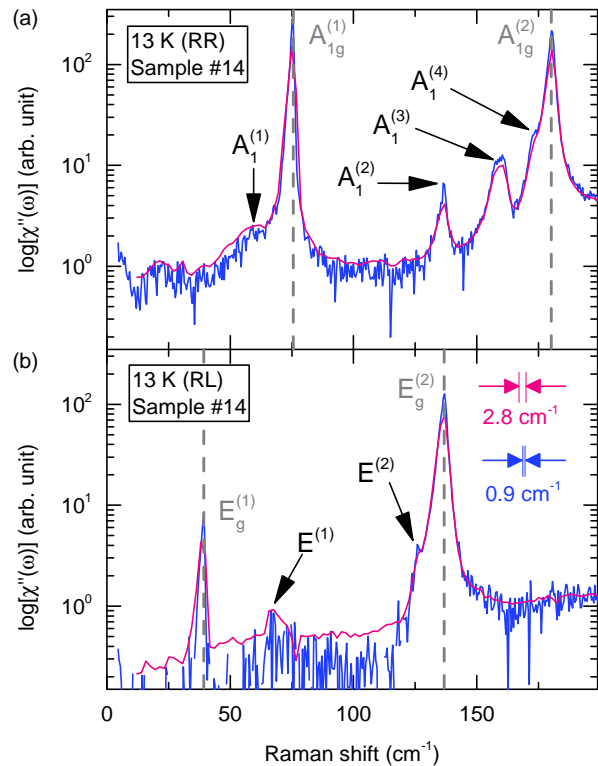


FIG. 4. (Color online) The Raman spectra taken in the (a) RR and (b) RL scattering geometry at 13 K with 532 nm excitation from a bulk Bi_2Se_3 single crystal are plotted on a semi-log scale. The red and blue curves correspond to instrumental resolution of 2.8 and 0.9 cm^{-1} (as shown in (b)), respectively. The bulk phonons are marked by gray dashed lines.

315 (0.9 cm^{-1}) spectra. Besides the more pronounced $A_1^{(2)}$
 316 and $A_1^{(3)}$ modes already visible in Fig. 3, we see a few additional
 317 features in the high resolution data: (1) A mode
 318 centered at 173 cm^{-1} appearing as a shoulder to the $A_{1g}^{(2)}$
 319 bulk phonon in RR geometry (Fig. 4(a)), which we designate
 320 as $A_1^{(4)}$. (2) Another mode centered at 126 cm^{-1}
 321 appearing as a shoulder to the $E_g^{(2)}$ bulk phonon in RL ge-
 322 ometry (Fig. 4(b)), which we designate as $E^{(2)}$. (3) The
 323 mode $A_1^{(3)}$ shows broadened peak structure. This cannot
 324 be due to splitting of an A -symmetry phonon, e.g.,
 325 lowering of symmetry, since A_1 is a one-dimensional rep-
 326 resentation. This can be explained as due to Fano inter-
 327 ference, which become more pronounced with infrared
 328 excitation (Fig. 2).

IV. DISCUSSION

331 At the crystal surface of Bi_2Se_3 , the lattice structure
 332 is distorted along c -axis due to the abrupt reduction of
 333 the interlayer van der Waals force that binds the crystal
 334 together, and is calculated by density functional theory

TABLE III. The summary of the bulk and surface phonon mode energies. This works data is compared to the spectroscopic studies reported in Ref. [30, 31, 33, 34, 37–42, 47, 51], and the calculations reported in Ref. [67, 73]. All values are given in units of cm^{-1} .

Symmetry	Experiment		Calculation	
	This work	Literature	LDA+SOI [67]	GGA+SOI [73]
$A_{1g}^{(1)}$	75	73 [31, 38, 40, 42]	77	64
$A_{1g}^{(2)}$	180	175 [31, 38, 40, 42]	176	167
$E_g^{(1)}$	39	39 [31, 38, 40, 42]	41	39
$E_g^{(2)}$	137	133 [31, 38, 40, 42]	139	124
$A_{2u}^{(1)}$	–	N/A	139	137
$A_{2u}^{(2)}$	–	N/A	161	156
$E_u^{(1)}$	–	61 [37]	80	65
$E_u^{(2)}$	–	133 [37]	131	127
$A_1^{(1)}$	60	68 [47]	N/A	N/A
$A_1^{(2)}$	136	129 [38]	N/A	N/A
$A_1^{(3)}$	158	160 [38, 51]	N/A	N/A
$A_1^{(4)}$	173	N/A	N/A	N/A
$E^{(1)}$	67	68 [38]	N/A	N/A
$E^{(2)}$	126	125 [38]	N/A	N/A

(DFT) to be about 10% along c -axis [47]. Additionally, the observation of two-dimensional electron gas formed on Bi_2Se_3 surface also supports the picture of subsurface van der Waals gap expansion [6, 74, 75]. However, finite phonon DOS exist across the entire energy range in Bi_2Se_3 [67], allowing the surface modes to decay into bulk phonon modes. Therefore, the surface mode is not entirely “peeled off” from the bulk. Instead, one would expect a “surface resonance” with slightly lower energy than the bulk phonon.

Due to inversion symmetry breaking at the crystal interface, the surface resonance from the Raman active A_{1g} and IR active A_{2u} phonons are both expected to appear in the A_1 symmetry (C_{3v} group), corresponding to out-of-plane atomic motion. The energies of such surface modes are usually slightly lower than the corresponding bulk phonons. This is consistent with the 4 A_1 modes we observed (Fig. 4(a)). From the energies of these A_1 modes, we conclude that $A_1^{(1)}$ and $A_1^{(4)}$ are associated with the bulk phonon modes $A_{1g}^{(1)}$ and $A_{1g}^{(2)}$, respectively. The measured energy of the $A_1^{(1)}$ mode is somewhat different than the previously reported value of 68 cm^{-1} by time resolved ARPES [47], but close to what was suggested by transport measurements [22]. We believe this difference may be partly due to surface quality variation. ARPES measured sample is usually cleaved in ultra high vacuum, whereas the surface in this study is cleaved in nitrogen environment. This may also explain why this mode was not observed in the MBE samples (Fig. 1), where the sample is unavoidably exposed to air for a few minutes during the transfer between MBE chamber and Raman cryostat. The $A_1^{(4)}$ mode appears as a shoulder

to the $A_{1g}^{(2)}$ bulk phonon, requiring higher resolution to distinguish from the bulk mode, and therefore was overlooked in the previous Raman study [38].

In comparison, the surface modes $A_1^{(2)}$ and $A_1^{(3)}$ have higher intensity and are better resolved. One possibility for this difference is that the bulk counterpart of these modes are the IR active $A_{2u}^{(1)}$ and $A_{2u}^{(2)}$ phonons, as the measured energy is close to the calculated values (Table III). Since these bulk modes are not Raman active, we were able to better resolve the surface resonance. Another possibility is that the phonon DOS is practically zero at these energies in the A_1 symmetry channel, and the surface vibration modes are truly localized. Distinguishing these two scenarios is in fact experimentally non-trivial, especially since the experimental values of the $A_{2u}^{(1)}$ and $A_{2u}^{(2)}$ bulk phonon energies are yet unknown.

Nevertheless, both possibilities point to the surface origin of these two modes, which provide us with information on the electron-phonon coupling at the TI surface. While the bulk phonons show little resonance effect, the $A_1^{(3)}$ phonon displays antisymmetric lineshape with 780 nm excitation, reminiscent of a Fano lineshape [76] (Fig. 2, inset). This was overlooked in previous Raman studies, and may be related to the 20 meV “kink” in the topological surface state’s energy dispersion curve reported by some ARPES measurements [49, 50]. The observation of Fano lineshape is a clear evidence for the existence of underlying electronic continuum in the A_1 symmetry channel, which interacts with the $A_1^{(3)}$ phonon [76, 77]. The excitation dependence also suggests resonance enhancement of the electronic continuum with near-infrared wavelength, consistent with the re-

ported surface states at about 1.6 eV above the Fermi energy [78, 79]. Fitting the 780 nm data with Eq. 4.48 in Ref. [77]:

$$I(\omega) = \frac{\pi\rho T_e^2(\omega_0 - \omega - VT_p/T_e)^2}{(\omega_0 - \omega + V^2R)^2 + (\pi V^2\rho)^2}, \quad (2)$$

yields electron-phonon interaction strength $V \approx 2.6 \text{ cm}^{-1}$, and phonon energy $\omega_0 \approx 158 \text{ cm}^{-1}$. Here we assumed the electron DOS ρ is a constant in the relevant energy window, and neglect the real part of the electronic Green's function R . T_p and T_e are the phonon and electronic continuum Raman transition matrix elements, respectively.

Since the in-plane symmetries are mainly preserved as the DFT calculated atomic surface distortion is purely out-of-plane [47], one would not expect surface phonon with E symmetry (C_{3v} group) for Bi_2Se_3 . However, the in-plane bonding potential is also modified by having distortion along c -axis, and therefore the phonon frequency at surface is still slightly different than the bulk value. If the modification is tiny, the E modes are expected to be weak and close to the bulk phonons. In Fig. 1(b) and Fig. 4(b), we can see hints of two additional modes, labeled by $E^{(1)}$ and $E^{(2)}$. The energies of these modes are in fact close to the measured values of $E_u^{(1)}$ and $E_u^{(2)}$ bulk phonons [36, 37], and are consistent with the previous Raman study [38] (Table III). However, the frequency of E_1 is slightly higher than $E_u^{(1)}$, which is against the expectation from a surface resonance. This may reflect the fact that this is an in-plane mode, orthogonal to the lattice distortion direction. Or, this may be indicative of non-trivial electron-phonon interaction with the surface states, and worth further studying.

V. CONCLUSION

In conclusion, we have done systematic symmetry analysis on the temperature and excitation dependent Raman spectra from high quality, freshly cleaved or grown ab surfaces of Bi_2Se_3 single crystal and films. We observed in total 4 out-of-plane, and possibly 2 in-plane surface vibrational modes, where we tabulate the energies and symmetries in Table III.

In particular, we reproduced the $A_1^{(1)}$ mode, which was previously observed in time resolved ARPES measurements [47]. The $A_1^{(1)}$ mode is interesting because it was found to couple strongly with the topological surface states, and therefore provides the main phononic decay channel for the Dirac fermions in Bi_2Se_3 . Our report of energies and symmetries of the $A_1^{(1)}$ and other surface modes affirms the validity of the surface lattice distortion model employed in Ref. [47]. The consistently much larger intensity for the out-of-plane vibration modes compared to in-plane modes strongly suggest that the surface lattice distortion and van der Waals gap expansion in Bi_2Se_3 is only along c -axis.

Lastly, the $A_1^{(2)}$ and $A_1^{(3)}$ modes have much stronger intensities compared to the other surface vibration modes, and may be candidates for localized surface phonons. In particular, we noticed the $A_1^{(3)}$ mode possesses a Fano lineshape in low doped Bi_2Se_3 single crystals. The Fano lineshape is indicative of electron-phonon coupling with the underlying electronic continuum of the same symmetry, important for understanding the relaxation and scattering of surface state excitations. Here, we found a resonance effect to the Fano lineshape with 780 nm excitation, suggesting the onset of the electronic continuum in A_1 symmetry has excitation dependence. This explains the inconsistent surface electron-phonon coupling constant found in previous ARPES studies [19, 46]. The excitation dependence also confirms the existence of unoccupied surface states at about 1.6 eV above the Fermi energy, which enhances the surface electronic continuum through resonance effect.

ACKNOWLEDGMENTS

G.B. and H.-H.K. acknowledge support from the U.S. DOE, BES grant DE-SC0005463. S.O., M.S., N.K. and M.B. are funded by Gordon and Betty Moore Foundation's EPiQS initiative (GBMF4418) and NSF(EFMA-1542798). S.-W.C. and X.W. acknowledge support from NSF Award DMREF-1233349. G.B. acknowledges partial support from QuantEmX grant from ICAM and the Gordon and Betty Moore Foundation through Grant GBMF5305.

Appendix: Removal of polarization leakage

In this section, we explain the details of data analysis concerning removal of polarization leakage from optical elements. The degree of leakage are determined from the $A_{1g}^{(1)}$ and $A_{1g}^{(2)}$ bulk phonons of single crystal samples at room temperature. The removal of polarization leakage is done by subtracting intensity from the orthogonal polarization geometry, i.e., $\chi''_{YX}(\omega) = \chi''_{YX}(\omega) - \alpha \cdot \chi''_{XX}(\omega)$, where $\chi''_{YX}(\omega)$ and $\chi''_{XX}(\omega)$ are raw data taken in YX and XX polarization geometries, respectively, and α is the leakage ratio due to the limitations of polarization optics. It is reasonable to suggest that the same ratio also applies to XX polarization geometry: $\chi''_{XX}(\omega) = \chi''_{XX}(\omega) - \alpha \cdot \chi''_{YX}(\omega)$. Similarly, we have $\chi''_{RL}(\omega) = \chi''_{RL}(\omega) - \beta \cdot \chi''_{RR}(\omega)$ and $\chi''_{RR}(\omega) = \chi''_{RR}(\omega) - \beta \cdot \chi''_{RL}(\omega)$ for the circularly polarized geometries, where β is the leakage ratio due to the limitations of the broadband quarter wave plate and alignment of the Berek compensator. The ratios α and β are in general a weak function of ω , but in a narrow energy window as in this study, they can be safely assumed as constants. In order to avoid confusion from contributions of surface phonons, we chose YX and RL geometries as our reference for determination of α and β . In these

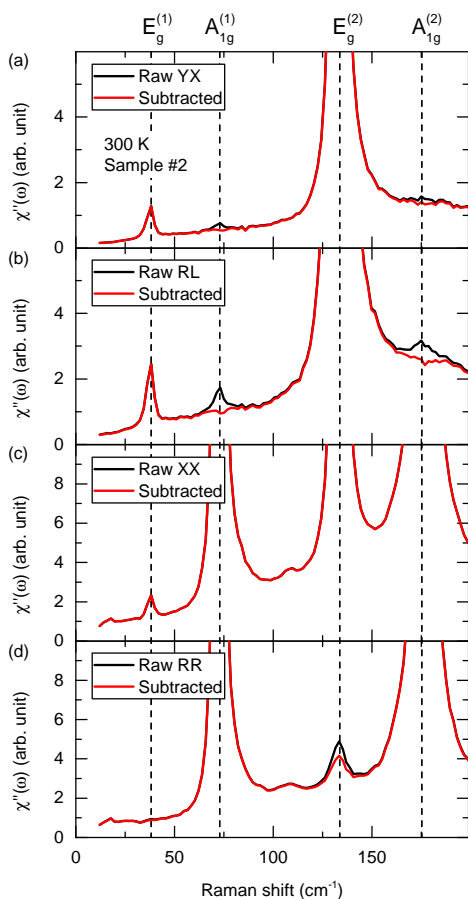


FIG. 5. (Color online) Comparison of raw data and polarization leakage removed spectra, taken in (a) YX, (b) RL, (c) XX, and (d) RR polarization geometry from the ab surface of Sample #2 at 300 K, with 532 nm excitation.

two geometries, only $E_g^{(1)}$ and $E_g^{(2)}$ bulk phonons are expected to be present, the E symmetry surface modes are extremely weak and close to the bulk phonons (Fig. 4), and therefore do not raise concern for determination of α and β .

In Fig. 5, we show spectra of unprocessed raw data and polarization leakage removed results taken at 300 K from the ab surface of a Bi_2Se_3 thick film in black and red lines, respectively. The leakage intensity of $A_{1g}^{(1)}$ and $A_{1g}^{(2)}$ bulk phonons in raw data taken with YX and RL geometries can be fully removed with leakage ratios $\alpha = 0.004$ and $\beta = 0.015$, respectively. These values are within the specification of used broadband polarization optics.

The value of α depends only on the wavelength of light, and therefore the same value $\alpha = 0.004$ is used for all samples and temperatures measured with 532 nm excitation. The value of β depends critically on the alignment of the Berek compensator, which may vary between experiments, and has to be determined using the method described above in each experiment. In this study, the value of β is always within the range 0.015 ± 0.005 .

-
- [1] Liang Fu, C. L. Kane, and E. J. Mele, “Topological insulators in three dimensions,” *Phys. Rev. Lett.* **98**, 106803 (2007).
- [2] Haijun Zhang, Chao-Xing Liu, Xiao-Liang Qi, Xi Dai, Zhong Fang, and Shou-Cheng Zhang, “Topological insulators in Bi_2Se_3 , Bi_2Te_3 and Sb_2Te_3 with a single Dirac cone on the surface,” *Nature Phys.* **5**, 438 (2009).
- [3] D. Hsieh, Y. Xia, D. Qian, L. Wray, J. H. Dil, F. Meier, J. Osterwalder, L. Patthey, J. G. Checkelsky, N. P. Ong, A. V. Fedorov, H. Lin, A. Bansil, D. Grauer, Y. S. Hor, R. J. Cava, and M. Z. Hasan, “A tunable topological insulator in the spin helical Dirac transport regime,” *Nature* **460**, 1101–1105 (2009).
- [4] Y. Xia, D. Qian, D. Hsieh, L. Wray, A. Pal, H. Lin, A. Bansil, D. Grauer, Y. S. Hor, R. J. Cava, and M. Z. Hasan, “Observation of a large-gap topological-insulator class with a single Dirac cone on the surface,” *Nature Phys.* **5**, 398–402 (2009).
- [5] J. G. Checkelsky, Y. S. Hor, M.-H. Liu, D.-X. Qu, R. J. Cava, and N. P. Ong, “Quantum interference in macroscopic crystals of nonmetallic Bi_2Se_3 ,” *Phys. Rev. Lett.* **103**, 246601 (2009).
- [6] Marco Bianchi, Dandan Guan, Shining Bao, Jianli Mi, Bo Brummerstedt Iversen, Philip D. C. King, and Philip Hofmann, “Coexistence of the topological state and a two-dimensional electron gas on the surface of Bi_2Se_3 ,” *Nat. Commun.* **1**, 128 (2010).
- [7] Haim Beidenkopf, Pedram Roushan, Jungpil Seo, Lindsay Gorman, Ilya Drozdov, Yew San Hor, R. J. Cava, and Ali Yazdani, “Spatial fluctuations of helical Dirac fermions on the surface of topological insulators,” *Nature Phys.* **7**, 939–943 (2011).
- [8] M. Zahid Hasan and Joel E. Moore, “Three-dimensional topological insulators,” *Annual Review of Condensed Matter Physics* **2**, 55–78 (2011).
- [9] Liang Fu and C. L. Kane, “Superconducting proximity effect and majorana fermions at the surface of a topological insulator,” *Phys. Rev. Lett.* **100**, 096407 (2008).
- [10] Xiao-Liang Qi, Taylor L. Hughes, and Shou-Cheng Zhang, “Topological field theory of time-reversal invariant insulators,” *Phys. Rev. B* **78**, 195424 (2008).
- [11] Xiao-Liang Qi, Rundong Li, Jiadong Zang, and Shou-

- Cheng Zhang, "Inducing a magnetic monopole with topological surface states," *Science* **323**, 1184–1187 (2009).
- [12] M. Z. Hasan and C. L. Kane, "Colloquium: Topological insulators," *Rev. Mod. Phys.* **82**, 3045–3067 (2010).
- [13] Rui Yu, Wei Zhang, Hai-Jun Zhang, Shou-Cheng Zhang, Xi Dai, and Zhong Fang, "Quantized anomalous hall effect in magnetic topological insulators," *Science* **329**, 61–64 (2010).
- [14] S. Raghu, Suk Bum Chung, Xiao-Liang Qi, and Shou-Cheng Zhang, "Collective modes of a helical liquid," *Phys. Rev. Lett.* **104**, 116401 (2010).
- [15] Xiao-Liang Qi and Shou-Cheng Zhang, "Topological insulators and superconductors," *Rev. Mod. Phys.* **83**, 1057–1110 (2011).
- [16] Y. H. Wang, H. Steinberg, P. Jarillo-Herrero, and N. Gedik, "Observation of Floquet-Bloch states on the surface of a topological insulator," *Science* **342**, 453–457 (2013).
- [17] Tarun Grover, D. N. Sheng, and Ashvin Vishwanath, "Emergent space-time supersymmetry at the boundary of a topological phase," *Science* **344**, 280–283 (2014).
- [18] N. P. Butch, K. Kirshenbaum, P. Syers, A. B. Sushkov, G. S. Jenkins, H. D. Drew, and J. Paglione, "Strong surface scattering in ultrahigh-mobility Bi_2Se_3 topological insulator crystals," *Phys. Rev. B* **81**, 241301 (2010).
- [19] Z.-H. Pan, A. V. Fedorov, D. Gardner, Y. S. Lee, S. Chu, and T. Valla, "Measurement of an exceptionally weak electron-phonon coupling on the surface of the topological insulator Bi_2Se_3 using angle-resolved photoemission spectroscopy," *Phys. Rev. Lett.* **108**, 187001 (2012).
- [20] T. Valla, Z.-H. Pan, D. Gardner, Y. S. Lee, and S. Chu, "Photoemission spectroscopy of magnetic and nonmagnetic impurities on the surface of the Bi_2Se_3 topological insulator," *Phys. Rev. Lett.* **108**, 117601 (2012).
- [21] V. Parente, A. Tagliacozzo, F. von Oppen, and F. Guinea, "Electron-phonon interaction on the surface of a three-dimensional topological insulator," *Phys. Rev. B* **88**, 075432 (2013).
- [22] M. V. Costache, I. Neumann, J. F. Sierra, V. Marinova, M. M. Gospodinov, S. Roche, and S. O. Valenzuela, "Fingerprints of inelastic transport at the surface of the topological insulator Bi_2Se_3 : Role of electron-phonon coupling," *Phys. Rev. Lett.* **112**, 086601 (2014).
- [23] I. M. Lifshitz and L. N. Rosenzweig, "Dynamics of lattice filling half-space (Russian)," *Zh. Eksp. Teor. Fiz.* **18**, 1012 (1948).
- [24] I. M. Lifshitz, "Some problems of the dynamic theory of non-ideal crystal lattices," *Il Nuovo Cimento* **3**, 716–734 (1956).
- [25] Richard F. Wallis, "Effect of free ends on the vibration frequencies of one-dimensional lattices," *Phys. Rev.* **105**, 540–545 (1957).
- [26] Richard F. Wallis, "Theory of surface modes of vibration in two- and three-dimensional crystal lattices," *Phys. Rev.* **116**, 302–308 (1959).
- [27] G. Benedek and L. Miglio, "The green's function method in the surface lattice dynamics of ionic crystals," in *Surface Phonons*, edited by Winfried Kress and Frederik W. de Wette (Springer Berlin Heidelberg, Berlin, Heidelberg, 1991) pp. 37–66.
- [28] R.F. Wallis, "Surface phonons: theoretical developments," *Surface Science* **299**, 612 – 627 (1994).
- [29] Maureen J. Lagos, Andreas Trügler, Ulrich Hohenester, and Philip E. Batson, "Mapping vibrational surface and bulk modes in a single nanocube," *Nature* **543**, 529–532 (2017), letter.
- [30] S. Y. F. Zhao, C. Beekman, L. J. Sandilands, J. E. J. Bashucky, D. Kwok, N. Lee, A. D. LaForge, S. W. Cheong, and K. S. Burch, "Fabrication and characterization of topological insulator Bi_2Se_3 nanocrystals," *Applied Physics Letters* **98**, 141911 (2011).
- [31] Jun Zhang, Zeping Peng, Ajay Soni, Yanyuan Zhao, Yi Xiong, Bo Peng, Jianbo Wang, Mildred S. Dresselhaus, and Qihua Xiong, "Raman spectroscopy of few-quintuple layer topological insulator Bi_2Se_3 nanoplatelets," *Nano Letters* **11**, 2407–2414 (2011).
- [32] V. Chis, I. Yu. Sklyadneva, K. A. Kokh, V. A. Volodin, O. E. Tereshchenko, and E. V. Chulkov, "Vibrations in binary and ternary topological insulators: First-principles calculations and Raman spectroscopy measurements," *Phys. Rev. B* **86**, 174304 (2012).
- [33] J. Humlíček, D. Hemzal, A. Dubroka, O. Čaha, H. Steiner, G. Bauer, and G. Springholz, "Raman and interband optical spectra of epitaxial layers of the topological insulators Bi_2Te_3 and Bi_2Se_3 on BaF_2 substrates," *Physica Scripta* **2014**, 014007 (2014).
- [34] Mahmoud Eddrief, Paola Atkinson, Victor Etgens, and Bernard Jusserand, "Low-temperature Raman fingerprints for few-quintuple layer topological insulator Bi_2Se_3 films epitaxied on GaAs," *Nanotechnology* **25**, 245701 (2014).
- [35] H. Köhler and C. R. Becker, "Optically active lattice vibrations in Bi_2Se_3 ," *physica status solidi (b)* **61**, 533–537 (1974).
- [36] W. Richter and C. R. Becker, "A Raman and far-infrared investigation of phonons in the rhombohedral V_2VI_3 compounds Bi_2Te_3 , Bi_2Se_3 , Sb_2Te_3 and $\text{Bi}_2(\text{Te}_{1-x}\text{Se}_x)_3$ ($0 < x < 1$), $(\text{Bi}_{1-y}\text{Sb}_y)_2\text{Te}_3$ ($0 < y < 1$)," *physica status solidi (b)* **84**, 619–628 (1977).
- [37] A. D. LaForge, A. Frenzel, B. C. Pursley, Tao Lin, Xinfei Liu, Jing Shi, and D. N. Basov, "Optical characterization of Bi_2Se_3 in a magnetic field: Infrared evidence for magnetoelectric coupling in a topological insulator material," *Phys. Rev. B* **81**, 125120 (2010).
- [38] V. Gnezdilov, Yu. G. Pashkevich, H. Berger, E. Pomjakushina, K. Conder, and P. Lemmens, "Helical fluctuations in the Raman response of the topological insulator Bi_2Se_3 ," *Phys. Rev. B* **84**, 195118 (2011).
- [39] Y. Kim, X. Chen, Z. Wang, J. Shi, I. Miotkowski, Y. P. Chen, P. A. Sharma, A. L. Lima Sharma, M. A. Hekmaty, Z. Jiang, and D. Smirnov, "Temperature dependence of Raman-active optical phonons in Bi_2Se_3 and Sb_2Te_3 ," *Applied Physics Letters* **100**, 071907 (2012).
- [40] Bushra Irfan, Satyaprakash Sahoo, Anand P. S. Gaur, Majid Ahmadi, Maxime J.-F. Guinel, Ram S. Katiyar, and Ratnamala Chatterjee, "Temperature dependent Raman scattering studies of three dimensional topological insulators Bi_2Se_3 ," *Journal of Applied Physics* **115**, 173506 (2014).
- [41] Yuan Yan, Xu Zhou, Han Jin, Cai-Zhen Li, Xiaoxing Ke, Gustaaf Van Tendeloo, Kaihui Liu, Dapeng Yu, Martin Dressel, and Zhi-Min Liao, "Surface-facet-dependent phonon deformation potential in individual strained topological insulator Bi_2Se_3 nanoribbons," *ACS Nano* **9**, 10244–10251 (2015).
- [42] Xin Zhang, Qing-Hai Tan, Jiang-Bin Wu, Wei Shi, and Ping-Heng Tan, "Review on the Raman spectroscopy of different types of layered materials," *Nanoscale* **8**, 6435–

- 6450 (2016).
- [43] Xuetao Zhu, L. Santos, R. Sankar, S. Chikara, C. Howard, F. C. Chou, C. Chamon, and M. El-Batanouny, “Interaction of phonons and Dirac fermions on the surface of Bi_2Se_3 : A strong Kohn anomaly,” *Phys. Rev. Lett.* **107**, 186102 (2011).
- [44] Xuetao Zhu, L. Santos, C. Howard, R. Sankar, F. C. Chou, C. Chamon, and M. El-Batanouny, “Electron-phonon coupling on the surface of the topological insulator Bi_2Se_3 determined from surface-phonon dispersion measurements,” *Phys. Rev. Lett.* **108**, 185501 (2012).
- [45] C. Howard, M. El-Batanouny, R. Sankar, and F. C. Chou, “Anomalous behavior in the phonon dispersion of the (001) surface of Bi_2Te_3 determined from helium atom-surface scattering measurements,” *Phys. Rev. B* **88**, 035402 (2013).
- [46] Richard C. Hatch, Marco Bianchi, Dandan Guan, Shining Bao, Jianli Mi, Bo Brummerstedt Iversen, Louis Nilsson, Liv Hornekær, and Philip Hofmann, “Stability of the Bi_2Se_3 (111) topological state: Electron-phonon and electron-defect scattering,” *Phys. Rev. B* **83**, 241303 (2011).
- [47] J. A. Sobota, S.-L. Yang, D. Leuenberger, A. F. Kemper, J. G. Analytis, I. R. Fisher, P. S. Kirchmann, T. P. Devereaux, and Z.-X. Shen, “Distinguishing bulk and surface electron-phonon coupling in the topological insulator Bi_2Se_3 using time-resolved photoemission spectroscopy,” *Phys. Rev. Lett.* **113**, 157401 (2014).
- [48] Z.-H. Pan, A. V. Fedorov, D. Gardner, Y. S. Lee, S. Chu, and T. Valla, “Measurement of an exceptionally weak electron-phonon coupling on the surface of the topological insulator Bi_2Se_3 using angle-resolved photoemission spectroscopy,” *Phys. Rev. Lett.* **108**, 187001 (2012).
- [49] Chaoyu Chen, Zhuojin Xie, Ya Feng, Hemian Yi, Aiji Liang, Shaolong He, Daixiang Mou, Junfeng He, Yingying Peng, Xu Liu, Yan Liu, Lin Zhao, Guodong Liu, Xiaoli Dong, Jun Zhang, Li Yu, Xiaoyang Wang, Qinjun Peng, Zhimin Wang, Shenjin Zhang, Feng Yang, Chuangtian Chen, Zuyan Xu, and X. J. Zhou, “Tunable Dirac fermion dynamics in topological insulators,” *Scientific Reports* **3**, 2411 (2013).
- [50] Takeshi Kondo, Y. Nakashima, Y. Ota, Y. Ishida, W. Malaeb, K. Okazaki, S. Shin, M. Kriener, Satoshi Sasaki, Kouji Segawa, and Yoichi Ando, “Anomalous dressing of Dirac fermions in the topological surface state of Bi_2Se_3 , Bi_2Te_3 , and Cu-doped Bi_2Se_3 ,” *Phys. Rev. Lett.* **110**, 217601 (2013).
- [51] A. Kogar, S. Vig, A. Thaler, M. H. Wong, Y. Xiao, D. Reig-i-Plessis, G. Y. Cho, T. Valla, Z. Pan, J. Schneeloch, R. Zhong, G. D. Gu, T. L. Hughes, G. J. MacDougall, T.-C. Chiang, and P. Abbamonte, “Surface collective modes in the topological insulators Bi_2Se_3 and $\text{Bi}_{0.5}\text{Sb}_{1.5}\text{Te}_{3-x}\text{Se}_x$,” *Phys. Rev. Lett.* **115**, 257402 (2015).
- [52] Norbert Esser and Wolfgang Richter, “Raman scattering from surface phonons,” in *Light scattering in solids VIII*, edited by Manuel Cardona and Gernot Güntherodt (Springer-Verlag, Berlin, 1999) pp. 96–168.
- [53] M. Liebhaber, U. Bass, P. Bayersdorfer, J. Geurts, E. Speiser, J. Räthel, A. Baumann, S. Chandola, and N. Esser, “Surface phonons of the $\text{Si}(111)-(7 \times 7)$ reconstruction observed by Raman spectroscopy,” *Phys. Rev. B* **89**, 045313 (2014).
- [54] P. LošTák, L. Beneš, S. Civiš, and H. Süssmann, “Preparation and some physical properties of $\text{Bi}_{2x}\text{In}_x\text{Se}_3$ single crystals,” *Journal of Materials Science* **25**, 277–282 (1990).
- [55] Jixia Dai, Damien West, Xueyun Wang, Yazhong Wang, Daniel Kwok, S.-W. Cheong, S. B. Zhang, and Weida Wu, “Toward the intrinsic limit of the topological insulator Bi_2Se_3 ,” *Phys. Rev. Lett.* **117**, 106401 (2016).
- [56] Matthew Brahlek, Namrata Bansal, Nikesh Koirala, Su-Yang Xu, Madhab Neupane, Chang Liu, M. Zahid Hasan, and Seongshik Oh, “Topological-metal to band-insulator transition in $(\text{Bi}_{1-x}\text{In}_x)_2\text{Se}_3$ thin films,” *Phys. Rev. Lett.* **109**, 186403 (2012).
- [57] Namrata Bansal, Yong Seung Kim, Matthew Brahlek, Eliav Edrey, and Seongshik Oh, “Thickness-independent transport channels in topological insulator Bi_2Se_3 thin films,” *Phys. Rev. Lett.* **109**, 116804 (2012).
- [58] M. Emziane, S. Marsillac, and J.C. Bernde, “Preparation of highly oriented $\alpha\text{-In}_2\text{Se}_3$ thin films by a simple technique,” *Materials Chemistry and Physics* **62**, 84 – 87 (2000).
- [59] McIver J. W., D. Hsieh, H. Steinberg, P. Jarillo-Herrero, and N. Gedik, “Control over topological insulator photocurrents with light polarization,” *Nat. Nanotechnol.* **7**, 96–100 (2012).
- [60] T. Terzibaschian and B. Enderlein, “The irreducible representations of the two-dimensional space groups of crystal surfaces. theory and applications,” *physica status solidi (b)* **133**, 443–461 (1986).
- [61] Jian Li, Jiufeng J. Tu, and Joseph L. Birman, “Symmetry predicted transitions in 3D topological insulators,” *Solid State Communications* **163**, 11 – 14 (2013).
- [62] Robert-Jan Slager, Andrej Mesaros, Vladimir Juricic, and Jan Zaanen, “The space group classification of topological band-insulators,” *Nature Phys.* **9**, 98–102 (2013).
- [63] R. Lewandowska, R. Bacewicz, J. Filipowicz, and W. Paszkowicz, “Raman scattering in $\alpha\text{-In}_2\text{Se}_3$ crystals,” *Materials Research Bulletin* **36**, 2577 – 2583 (2001).
- [64] L. N. Ovander, “The form of the Raman tensor,” *Opt. Spectrosc.* **9**, 302 (1960).
- [65] Manuel Cardona, “Resonance phenomena,” in *Light scattering in solids II*, edited by Manuel Cardona and Gernot Güntherodt (Springer-Verlag, Berlin, 1982) pp. 45–49.
- [66] G.F. Koster, *Properties of the thirty-two point groups*, Massachusetts institute of technology press research monograph (M.I.T. Press, 1963).
- [67] Bao-Tian Wang and Ping Zhang, “Phonon spectrum and bonding properties of Bi_2Se_3 : Role of strong spin-orbit interaction,” *Applied Physics Letters* **100**, 082109 (2012).
- [68] Yuri D Glinka, Sercan Babakiray, Trent A Johnson, and David Lederman, “Thickness tunable quantum interference between surface phonon and Dirac plasmon states in thin films of the topological insulator Bi_2Se_3 ,” *Journal of Physics: Condensed Matter* **27**, 052203 (2015).
- [69] Liang Wu, M. Brahlek, R. Valdes Aguilar, A. V. Stier, C. M. Morris, Y. Lubashevsky, L. S. Bilbro, N. Bansal, S. Oh, and N. P. Armitage, “A sudden collapse in the transport lifetime across the topological phase transition in $(\text{Bi}_{1-x}\text{In}_x)_2\text{Se}_3$,” *Nature Phys.* **9**, 410–414 (2013).
- [70] Hang Dong Lee, Can Xu, Samir M. Shubeita, Matthew Brahlek, Nikesh Koirala, Seongshik Oh, and Torgny Gustafsson, “Indium and bismuth interdiffusion and its influence on the mobility in $\text{In}_2\text{Se}_3/\text{Bi}_2\text{Se}_3$,” *Thin Solid Films* **556**, 322 – 324 (2014).

- [71] B. S. Shastry and B. I. Shraiman, “Raman Scattering in Mott-Hubbard Systems,” *Int. J. Mod. Phys. B* **5**, 365–388 (1991).
- [72] D. V. Khveshchenko and P. B. Wiegmann, “Raman scattering and anomalous current algebra in mott insulators,” *Phys. Rev. Lett.* **73**, 500–503 (1994).
- [73] Wei Cheng and Shang-Fen Ren, “Phonons of single quintuple Bi_2Te_3 and Bi_2Se_3 films and bulk materials,” *Phys. Rev. B* **83**, 094301 (2011).
- [74] Marco Bianchi, Richard C Hatch, Dandan Guan, Tilo Planke, Jianli Mi, Bo Brummerstedt Iversen, and Philip Hofmann, “The electronic structure of clean and adsorbate-covered Bi_2Se_3 : an angle-resolved photoemission study,” *Semiconductor Science and Technology* **27**, 124001 (2012).
- [75] T. V. Menshchikova, S. V. Eremeev, and E. V. Chulkov, “On the origin of two-dimensional electron gas states at the surface of topological insulators,” *JETP Letters* **94** (2011).
- [76] U. Fano, “Effects of configuration interaction on intensities and phase shifts,” *Phys. Rev.* **124**, 1866–1878 (1961).
- [77] M.V. Klein, “Electronic raman scattering,” in *Light Scattering in Solids I*, edited by M. Cardona and G. Güntherodt (Springer-Verlag, Berlin, 1983) pp. 169–172.
- [78] J. A. Sobota, S.-L. Yang, A. F. Kemper, J. J. Lee, F. T. Schmitt, W. Li, R. G. Moore, J. G. Analytis, I. R. Fisher, P. S. Kirchmann, T. P. Devereaux, and Z.-X. Shen, “Direct optical coupling to an unoccupied Dirac surface state in the topological insulator Bi_2Se_3 ,” *Phys. Rev. Lett.* **111**, 136802 (2013).
- [79] D. Niesner, Th. Fauster, S. V. Eremeev, T. V. Menshchikova, Yu. M. Koroteev, A. P. Protogenov, E. V. Chulkov, O. E. Tereshchenko, K. A. Kokh, O. Alekperov, A. Nadjafov, and N. Mamedov, “Unoccupied topological states on bismuth chalcogenides,” *Phys. Rev. B* **86**, 205403 (2012).